Sputtering deposition under limited adatom mobility: an effective method to prepare a SERS substrate based on Ag@ZnO composite deposited onto electrospun cellulose acetate fibers

Adrián Camacho-Berríos [1], Oscar Marcelo Suárez [1]

Department of Engineering Sciences and Materials, [1]University of Puerto Rico - Mayagüez, Puerto Rico, USA

Corresponding author email: adrian.camacho@upr.edu

Abstract: Sputtering is a well-known physical vapor deposition method for the synthesis of coatings and thin films. When combined with other techniques, such as electrospinning, it becomes a straightforward yet effective method to prepare substrates that can render various morphological structures at the nano and micrometer scale. The resulting substrates possess high surface area, making them suitable for applications such as gas sensing and surface-enhanced Raman scattering (SERS). The present work reports the successful magnetron sputtering deposition of silver/zinc oxide (Ag@ZnO) onto cellulose acetate fibers. By adjusting the sputtering process parameters, we limited the deposition of ZnO and Ag to be under limited adatom mobility conditions. Secondary electron imaging revealed that the resulting ZnO morphology on the fibers presented a columnar grain morphology at the nanometer scale. The ZnO crystallites of the said grains possessed a wurtzite structure, as shown by Raman spectroscopy. Ag sputtering deposition onto the previously deposited ZnO-covered fibers, produced under limited adatom mobility and short deposition time, rendered nanoparticles of various shapes and sizes, as revealed by electron microscopy. Then, using benzenethiol (BZT) and rhodamine 6G (R6G) as the probe molecules, the Ag@ZnO/CA fibers were tested as SERS substrates. All the prepared composite materials showed good SERS response towards the BZT and R6G. In summary, the novel approach is a practical and straightforward route for preparing Ag/ZnO-based SERS substrates.

Keywords: Sputtering, Ag@ZnO composite, SERS, cellulose acetate fibers

Acknowledgments

This work was supported by the National Science Foundation grants number 2112537 (NSF CREST Postdoctoral Research Fellowship) and 1345156 (NSF CREST Program). Infrastructure support by the UPRM Dean of Students Office is acknowledged by coauthor Suárez. The authors would like to thank the Material Characterization Center of the University of Puerto Rico (UPR) for electron microscopy services and Dr. Danilo Barrionuevo (UPR- Cayey campus) for his assistance in the profilometer measurements. The authors acknowledge the UPR-Cayey campus for the sputtering facilities. The authors acknowledge the UPR Molecular Science Research Center for the Raman and SERS measurements. We also kindly acknowledge Professors Marco De Jesus and Francisco Bezares for many helpful discussions about SERS. The authors would like to thank Dr. Wilfredo for his valuable and constructive suggestions during the revision process of the manuscript.

Adrian Camacho Berrios (ORCID 0000-0002-1673-1663)

Oscar Marcelo Suarez (ORCID 0000-0002-3797-4787)

1 Introduction

As an analytical technique, Surface-enhanced Raman Scattering (SERS) is of great interest to researchers for its potential applications in various fields such as environmental science [1,2], food safety [3,4], agriculture [5], and forensic sciences [6,7], due to its ability to detect molecules at trace levels. In SERS, the characteristic vibrational modes of a molecule can be identified from the interaction between the electromagnetic radiation and the molecule being studied [8]. This is similar to Raman scattering, although SERS signals are enhanced several orders of magnitude. The origin of this enhancement lies in the physical properties of the substrates. These substrates are typically metals where charge density oscillations couple resonantly with the electromagnetic radiation forming a surface plasmon, for continuous metal surfaces, or a localized surface plasmon (LSP) for metallic nanoparticles [9]. Surface plasmons (continuous or localized) and the lightning rod effect contribute to the electromagnetic (EM) enhancement mechanism, one of the two main enhancement mechanisms known in SERS, the other one being the chemical enhancement mechanism [10].

Early studies on metallic nanoparticles showed that the SERS effect could be optimized by tuning the size and shape of the nanoparticles. For instance, Barbosa et al. [11], tuned the LSP resonance frequency of star-shaped Au nanoparticles by changing their dimensions. Similarly, Zhang et al. [12], demonstrated that the LSP could be tuned by controlling the thickness and shape of the Ag nanoplates. Another aspect of shapes such as nanostars and nanoplates is the occurrence of tips and sharp edges that can concentrate electromagnetic radiation, contributing to EM enhancement, as indicated by Barbosa. The extra enhancement is also attributed to tips in other shapes, such as popcorn-like nanoparticles [13]. Despite the advantage of easy preparation and tunable optical properties, the agglomeration of the nanoparticles is a significant drawback for practical applications because they can be randomly organized, making it challenging to control them, therefore, affecting the reproducibility of those experiments.

The agglomeration problem was offset by fabricating highly oriented arrays of metallic nanostructures on rigid substrates [14–16]. One example is the dimmer-based optical antennas fabricated by Zhu et al. [16]. These antennas are made of an array of dimers fabricated on an indium tin oxide-coated glass via e-beam lithography. This method allows for the precise control of the dimmer size and the gap between the dimers where the EM field is intense. These authors also fabricated antennas with gaps between the dimers as small as 3 nm allowing for a high SERS response. Like the tips and sharp edges of the nanoparticles, gaps play an essential role as the EM field within the nanoparticles provide a considerable EM enhancement compared to an isolated nanoparticle [17]. Although these nanostructures show high SERS performance, their practical application can be limited by their production methods since they can be expensive, time-consuming, and technically challenging.

Metal oxide composite-based SERS substrates such as copper(II) oxide Nanowires/ copper(I) oxide (CuO Nanowires/Cu_2O) [18], silver/zinc oxide (Ag@ZnO) [19], and gold/zinc oxide (Ag@ZnO) [20] composites have the potential to overcome the abovementioned difficulties and have also attracted attention due to their multifunctional properties. Compared to SERS substrates based on pure metallic nanoparticles, metal-metal oxide composite based on Ag@ZnO or Au@ZnO inherit their multifunctionality from the ZnO properties, in addition to displaying high SERS enhancement [21], low detection limit of probe molecules [22,23], and good SERS signal uniformity [20,24]. For example, a porous ZnO layer covering the Au nanoparticles can provide adsorption sites for gas molecules to detect benzene-volatile organic compounds [25]. Furthermore, the said layer contributes to the SERS signal through the chemical enhancement mechanism. Additionally, ZnO photocatalytic properties are known for helping develop recyclable or reusable SERS substrates [19,22,26,27]. In the past decade, researchers have prepared these composites in remarkable morphologies like nanoneedles arrays [28], nanorods

arrays [29,30], nanodomes [31], nanomaces [32], multipods [27], nanoflowers [33], fibers [34,35] and nanofibers [36]. Specifically, fiber-based SERS substrates are very interesting for fabricating wearable SERS optical sensors [37].

Different methods have been applied to fabricate Ag@ZnO, Au@ZnO fibers, and nanofibers. Most combine techniques such as hydrothermal, electrospinning, and sputtering. For example, Park et al. worked on electrospun Ag@ZnO nanofibers using polyvinyl alcohol (PVA) and metal-polymer precursors followed by thermal treatments [36]. Fang Lu et al. [38] combined electrospinning with hydrothermal and photoreduction processes to synthesize Ag nanoparticles on ZnO nanorods grown on polyimide/Ag nanofibers. Other methods rely on the use of sputtering deposition either alone or in combination with another technique. For example, a hydrothermal method was used to prepare ZnO nanorods on a stainless-steel fiber decorated with Au nanoparticles deposited by ion sputtering [35]. Yuan et al. sputtered Ag/ZnO thin films on polyester fibers [34]. In summary, different combinations of techniques were available to prepare Ag@ZnO on nanofibers. Nonetheless, little attention has been paid to the sputtering deposition of both constituents of the composite onto the fibers.

Combining sputtering deposition and electrospinning turns into a simple and effective method for fabricating substrates that yield high surface area and interesting morphological structures where the fibers are used as scaffolds. By adjusting the sputtering process parameters, the morphological structures can be varied at the micro and nanoscale. For example, Pantojas et al. [39] prepared palladium nanoshells by sputtering palladium onto electrospun polyethylene oxide (PO) nanofibers. After the sputtering deposition, they heated the samples in air to remove the PO nanofibers. By tuning the sputtering parameters, these authors modified three types of structures within the palladium nanoshells: the columnar structure, the shape of the nanoshell walls, and their crystallinity. The shape of the nanoshell walls could change from nanoribbons to fully formed tubes by increasing the sputtering time such that the sputtered material covered the PO nanofibers completely. Under low adatom mobility conditions (e.g., low substrate temperature and relatively high sputtering pressure), the palladium nanoshells had columnar grains. This approach is suitable for substrates with a high surface area that could be used in many applications, such as gas sensing and SERS.

In the present work, we follow the ideas presented by Pantojas et al. and extend them to the sputtering deposition of ZnO and Ag onto cellulose acetate (CA) fibers. By adapting the said technology, we have successfully prepared an Ag@ZnO composite magnetron-sputtered onto electrospun CA fibers (Ag@ZnO/CA fibers) under low adatom mobility conditions. Our work offers a facile approach to produce Ag@ZnO/CA fibers that can be used as SERS sensors for various applications. This research also provided insight into the effects of limited adatoms mobility conditions on the morphology and optical properties of Ag@ZnO/CA fibers. The resulting composite fibers were tested as a SERS substrate using benzenethiol (BZT) and rhodamine 6 G (R6G) as probe molecules.

2 Methodology

The present study aims to prepare an Ag@ZnO composite sputtered onto electrospun CA fibers that were subsequently tested as SERS substrates using BZT. Preparing the composite structure comprised three steps: (a) the synthesis of the cellulose acetate fibers; (b) the ZnO sputtering deposition onto the AC fibers, and (c) the Ag sputtering deposition onto the ZnO-fiber composite. The following sections describe the methodology and the characterization used in this work.

2.1 Synthesis of cellulose acetate fibers

We first dissolved cellulose acetate powder into a mixture of dimethylformamide (DMF), ethanol, and acetone to synthesize the CA fibers preparation. Subsequently, we magnetically stirred the solution overnight to obtain a homogeneous one. Then, the solution was electrospun using a laboratory-made electrospinning system under a potential difference of 20 kV and a 0.5 ml/h flow rate. Finally, we collected the fibers onto 1 cm^2 glass slides placed on a collector.

2.2 ZnO sputtering

A reactive direct current (DC) magnetron sputtering deposited a ZnO layer on the cellulose acetate fibers. The fibers were placed in a $1.3x10^{-4}$ Pa pressure chamber. For the ZnO sputtering, we used a 50.8 mm metallic Zn target at 6 cm from the substrate. Before the sputtering deposition of ZnO, the Zn target was pre-sputtered in an Ar atmosphere for 120 s to clean the target and do the depositions in the metallic mode. A 1.3 Pa pressure, using Ar and oxygen as reactive gas, and 100 W sputtering power were used for the deposition. The oxygen-to-argon flow ratio and the sputtering deposition time were set at 30 % and 600 s, respectively.

2.3 Sputtering deposition of Ag

We silver-coated the ZnO/CA fibers via DC magnetron sputtering. The deposition was carried out under an Ar atmosphere of 1.7 Pa, using a 25.4 mm diameter Ag target and 50 W of sputtering power. The target-to-substrate distance was 6.5 cm, and the sputtering times were 5, 10, and 15 s. All the sputtering depositions were carried out without intentionally heating the substrate.

2.4 Characterization of the substrates

A masked silicon substrate, included alongside the CA fibers during the sputtering deposition, was used to create a ZnO step that was measured using a stylus profilometer to obtain the deposited thickness. The ZnO layer thickness was measured as a function of the sputtering time. The deposition rate was estimated by dividing the layer thickness by the sputtering deposition time. The same procedure was followed to determine the Ag deposition rate. The morphology and elemental composition were evaluated using a scanning electron microscope with an energy-dispersive spectroscopy module. As the Ag deposited on the ZnO/CA fibers can suffer from oxidation due to the ambient conditions and thus reduce the performance of the SERS substrate, we stored the samples in a vacuum desiccator under partial vacuum conditions until each characterization. For the BZT SERS measurements, a Raman microscope (Thermo Fisher Scientific Inc, USA), with an excitation source of 532 nm. All the spectra were obtained using a 10x objective lens with a 5 mW laser power and 5 s exposure time with two accumulations. To minimize the fluorescence effect of the R6G molecules on the SERS spectra, we used 0.5 mW power to collect the R6G spectra with 2 s exposure time and eight acquisitions. The SERS spectra were baseline-corrected Asymmetric Least Square Smoothing. The peaks were fitted using the Multi-Peak Fitting package from Igor Pro (WaveMetrics, Lake Oswego, OR, USA), with Gaussian shape peaks and a constant function baseline.

3. Results and discussion

3.1 Sputtering deposition of ZnO onto the CA fibers

The magnetron sputtering technique will permit the deposition of ZnO on cellulose nanofibers [40–44]. Sputtering is a widely used coating technique where through a cold plasma glow discharge and gas ion bombardment onto the target material's surface; atoms are sputtered on a substrate [45]. With this technique, one can make coatings of any material, including compounds such as ZnO. One way to prepare compounds is reactive sputtering [41]. The ZnO's deposition by reactive sputtering using a Zn target has

some advantages compared to the direct sputtering from a ZnO target. Firstly, Zn targets have higher purity than ZnO targets. ZnO targets are made by hot pressing and sintering powder; during this process, gases, porosity, and impurities are incorporated into the target, reducing its purity [45]. Secondly, considerable changes in the composition and properties of the reactively sputtered films from metallic targets are possible, depending on processing parameters such as the amount of reactive gas [44,46]. Thus, the first step to prepare the Ag@ZnO composite with a fiber morphological structure was the ZnO deposition onto the CA fibers. We deposited ZnO from a Zn target onto the electrospun CA fibers that served as scaffolds. Fig. 1 shows the average thickness of ZnO thin films as a function of the deposition time obtained from profilometry. For the sputtering parameters used in this work, the ZnO deposition rate was around 18.3 nm/min, as obtained from a linear fitting of two data points and the origin.

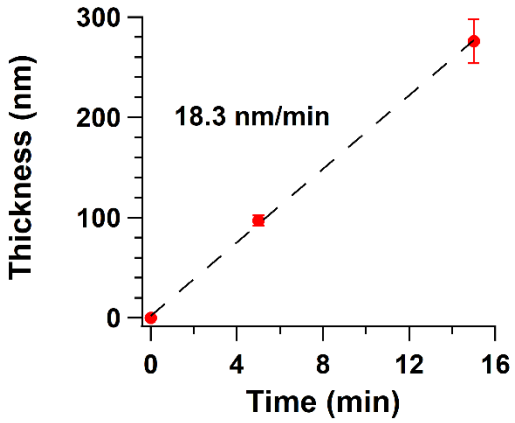

Fig. 1 The sputtering deposition rate of thin films grown on a Si substrate by reactive magnetron sputtering using a DC power supply at 30 % O_2/(Ar+O_2) flow ratio. The two data points are means ± 1 standard error (SE) (n=5)

Next, we evaluated the surface morphology and elemental composition of the sputtered material on the CA fibers using Scanning Electron Microscopy (SEM) and Energy Dispersive Spectroscopy (EDS), respectively. The SEM micrographs (Fig. 2a) show the entwined CA fibers after the reactive DC magnetron sputtering at a 30% O_2/(Ar+O_2) flow ratio for a 900 s deposition, corresponding to 200 nm thickness of sputtered material. As expected, the EDS results show the presence of Zn and O characteristic transition energies suggesting the possible formation of ZnO on the CA fibers. Fig. 3a shows a high-magnification SEM micrograph of a fiber. The structure of the sputtered layer consists of nanoscaled columnar grains covering the top of the fibers with a top dome morphology typical of zone 1 of the structure-zone models of Thornton [39] and Messier [40]. Sputtering is a line-of-sight deposition process [38], and the fiber is a variable-angle surface. The thickness of ZnO deposited on top of the CA fiber is expected to be around 200 nm, the same as the flat Si surface. But, at the edges of the fibers, the amount of material deposited will be smaller, and shadowing will tend to separate the columns. On the top of the CA fibers, the dome diameter averaged 54.7 nm for the middle section (estimated using ImageJ software tools), as shown in Fig. 3b. ZnO columns, 200nm of height and ~ 50 nm diameter on top are expected in the top midsection of the fiber, while smaller height columns with a wider spread, should come forth at the edges of the CA fibers.

The structure of the sputtered material is linked to the mobility of the atoms absorbed on the surface of the growing film. In the structure-zone model proposed by Thornton [47], the film structure results from many concurrent processes (i.e., surface diffusion, bulk diffusion, and desorption). The homologous temperature T_m (i.e., the ratio between the substrate temperature and the melting point of the growing material) and the sputtering gas pressure are dominant mechanisms during film growth. The model was

extended by Messier [48] to account for bombardment-induced mobility, thermal effects, and the evolution of the growing film at low mobility conditions. In the present work, the sputtering of ZnO was carried out by avoiding heating the substrate, which remained at 300 K, and no electrical biasing of the substrate. Thus, using the melting temperature of 2248 K [49] for ZnO and a substrate temperature of 300 K, the homologous temperature is $T_m = 0.1$, corresponding to Zone 1 of the structure-zone models. At an extremely low T_m, the surface mobility due to thermal effects is negligible; as a result, the microstructure in Zone 1 consists of columnar grains. In addition, these columns have poor crystallinity and voids between them. The full coverage observed on the CA fiber (Fig. 3a) by the sputtered layer could be explained by considering the sputtering time, the deposition pressure, and the power used. An advantage of the combined fiber morphology and columnar grain structure of the sputtered layers, topped in a dome surface morphology, is the abundance of surface area for the analyte to be absorbed and, therefore, be detected using SERS.

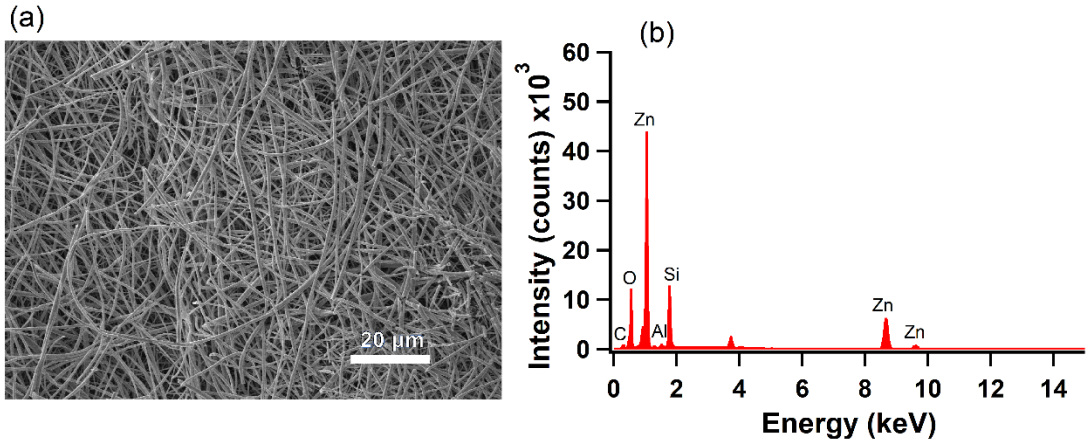

Fig. 2 SEM image (**a**) and EDS spectra (**b**) of the ZnO/CA fibers substrates

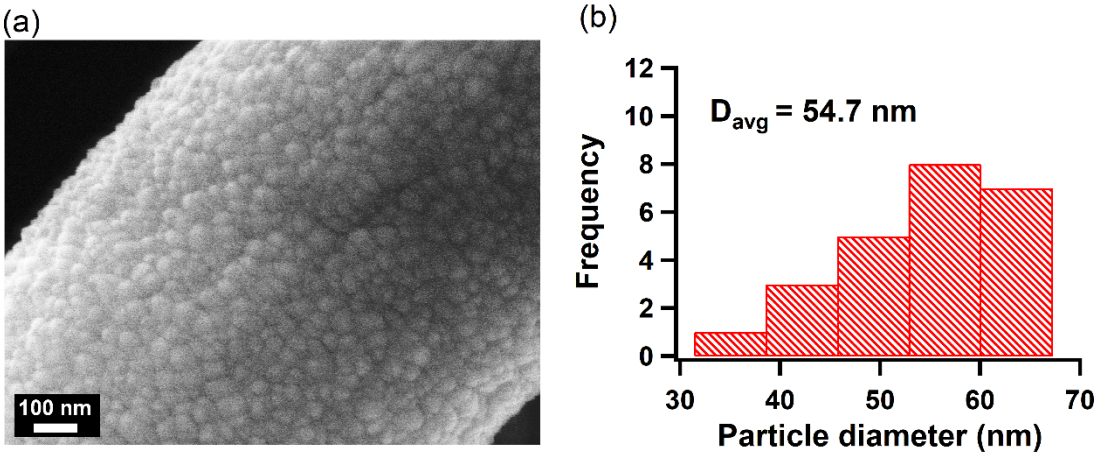

Fig. 3 High magnification SEM image of ZnO deposited on CA (**a**); particle diameter distribution (**b**). The number of bins in the histogram and their width are 5 and 7.7, respectively

Fourier-transform infrared spectroscopy (FTIR) and Raman spectroscopy are valuable techniques for identifying crystalline structures. Fig. 4a shows the FTIR spectra of the as-spun CA and CA fibers after the reactive DC sputtering deposition. We can identify the vibrational features of cellulose acetate and wurtzite ZnO from the spectra. The 1,743 cm^{-1} and 1,226 cm^{-1} bands are assigned to the vibrational modes

of cellulose acetate [50]. The band between 500 cm^{-1} and 600 cm^{-1} is ascribed to the stretching mode of the Zn-O bond in the ZnO lattice [51].

Fig. 4b shows the Raman spectra of CA and ZnO/CA. As seen in Fig. 4b, the intensities of the CA peaks are attenuated, whereas three peaks become apparent in the 60-1000 cm^{-1} range after the sputtering deposition of ZnO. These predominant peaks are around 97 cm^{-1}, 435 cm^{-1}, and 580 cm^{-1}. The assignment of the peak identity was made following the published literature [52]. The peak near 97 cm^{-1} is assigned to the E_2 (low) phonon mode, and the 435 cm^{-1} peak corresponds to the E_2(high) phonon mode of ZnO with the wurtzite crystal structure.

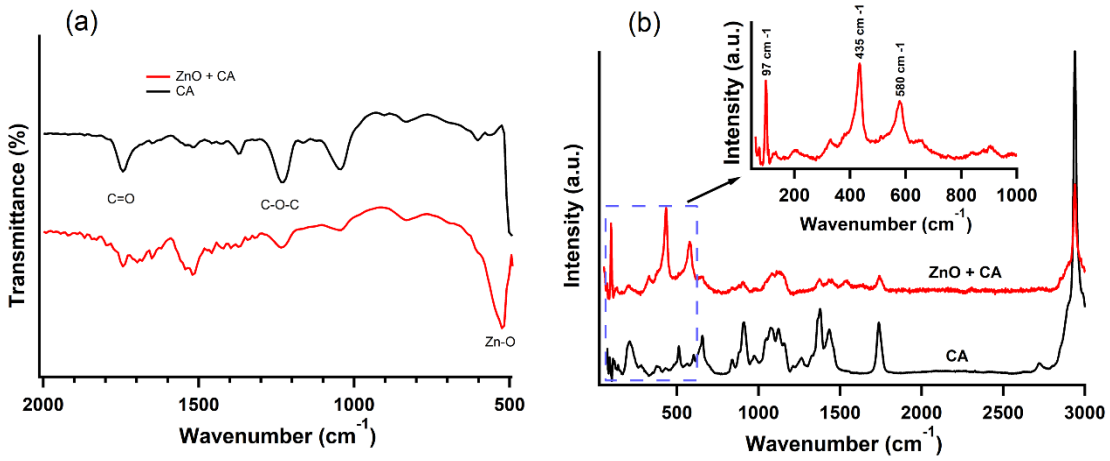

Fig. 4 FT-IR spectra for CA fibers (black) and ZnO/CA fibers (red) (**a**). The peak near 524 cm^{-1} indicates the vibrational stretching mode of the Zn-O bond in the ZnO lattice. Raman spectra of the CA fibers (black) and for the ZnO/CA fibers (**b**). The peaks near 97 cm^{-1} and 435 cm^{-1} are characteristic of the ZnO wurtzite structure

The peak near 580 cm^{-1} has been ascribed to the A_1(Low) [53,54] or the E_1(Low) [55,56] phonon modes. These modes are attributed to ZnO lattice defects [48,49] . Because we are depositing ZnO from a metallic Zn target by adding a relatively small amount of oxygen to the sputtering gas mixture, the occurrence of oxygen vacancies in the ZnO lattice is likely. Consequently, the observed 580 cm^{-1} peak can be associated with the phonon mode that arises from oxygen vacancies in the ZnO lattice. Clearly, the FTIR and Raman results confirm the wurtzite ZnO deposition onto the CA fibers.

3.2 Sputtering deposition of Ag

As in the ZnO deposition, Ag was sputtered onto the ZnO/CA fibers under limited adatom mobility conditions. The substrate temperature remained at 300 K, and the power was set to 50 W to minimize the bombardment-induced adatom mobility. At pressures above 1 Pa, scattering events of the sputtered atoms with neutrals and ions in the plasma reduce their induced mobility when they arrive to the substrate. Thus, considering this effect, we selected a pressure of 1.7 Pa for the Ag deposition onto the ZnO/CA fibers.

Chang et al. [58], used ion-beam sputtering for the deposition of Ag nanoparticles on ZnO:Al nanoneedles, observed that by extending the sputtering deposition time, the Ag nanoparticles size and surface coverage gradually increased until Ag film completely covered the nanoneedles. However, they did not behave similarly for the SERS intensity as a function of the sputtering time. The SERS intensity first rose to a maximum and decreased at longer sputtering times. Thus, to assess the sputtering time effect on the Ag surface morphology and the compound SERS intensity, we sputtered Ag onto the ZnO/CA nanofibers at 5, 10, and 15 seconds.

The morphology and elemental composition of the ZnO/CA fibers decorated with Ag at different deposition times were examined with SEM and EDS, respectively. Fig. 5 shows the low magnification SEM image (inset Fig. 5) and EDS spectrum of the Ag@ZnO/CA fibers sputtered with Ag for 5 seconds. The appearance of their respective peaks confirms the constituent elements for Ag@ZnO, Zn, O, and Ag. Fig. 6 shows the high magnification micrographs of Ag on the ZnO/CA fibers as deposited by DC sputtering at various deposition times: (a) 5 s, (b) 10 s, (c) 15 s, (d) 20 s and (e) 25s. As shown in Fig. 6a, at five seconds, the resulting Ag morphology consists of nanoparticles of different shapes and sizes distributed on top and along the ZnO/CA fiber surface. Albeit, at 10, 15, 20 and 25 seconds, the Ag surface coverage of the surface of ZnO/CA fibers increased promptly, rendering a more continuous Ag film. Interestingly, this result, i.e., the expedited rising of surface coverage, contrasts with the gradual increase in surface coverage reported by Chang et al. The difference could be related to the sputtering parameters used in their experiment or the orientation between the nanoneedle surface and the incoming flux of sputtered material.

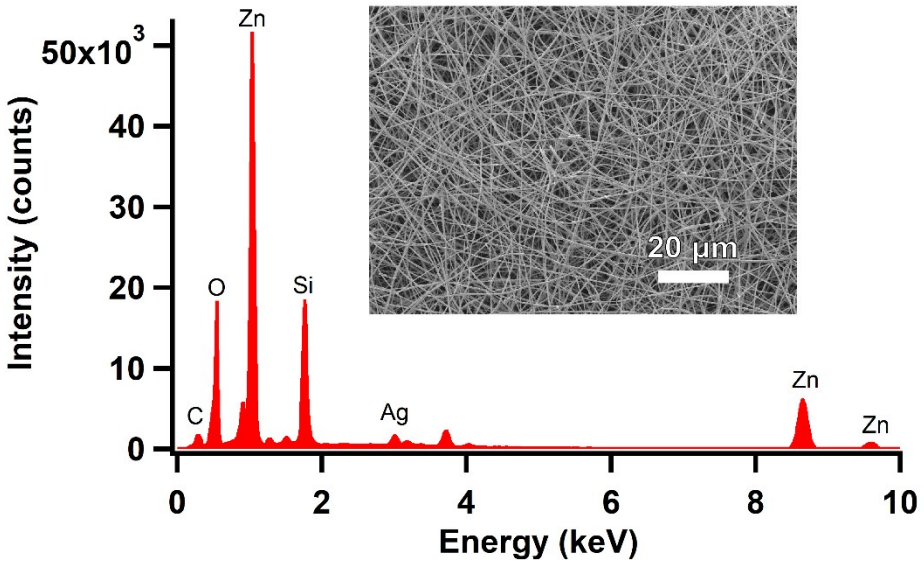

Fig. 5 EDS spectra and low magnification SEM image of Ag@ZnO/CA fibers substrates. The EDS spectrum confirms the presence of Ag in Ag@ZnO with Ag deposition for 5 s

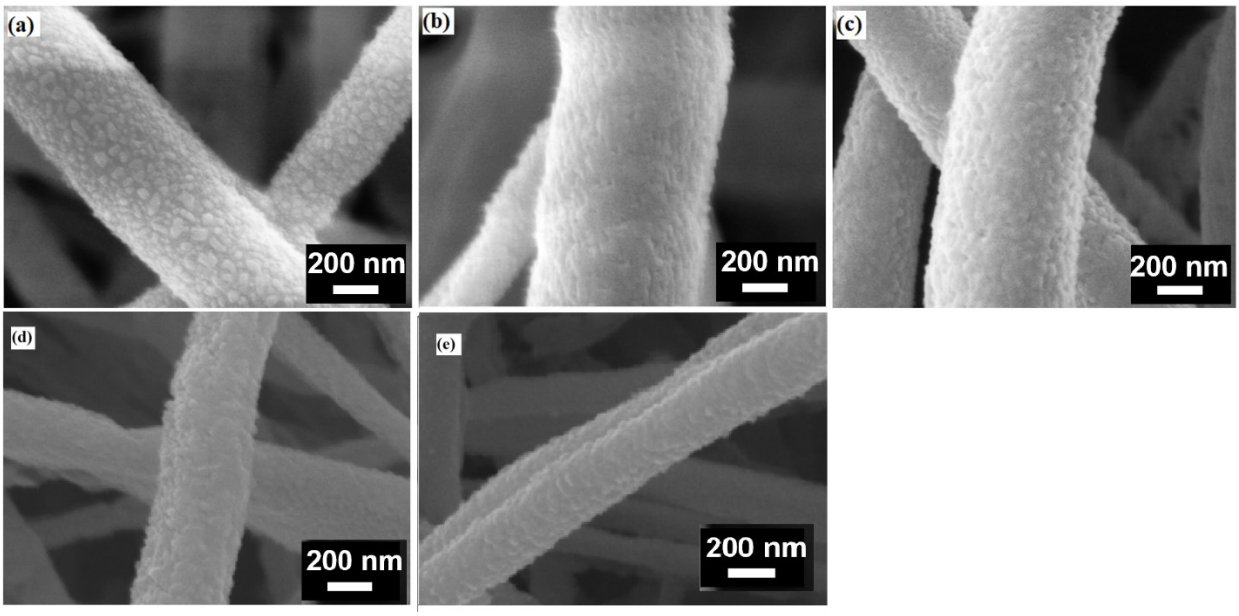

Fig 6 High magnification SEM micrographs of Ag@ZnO/CA fibers/glass substrates after depositing Ag at 5 s (**a**), 10 s (**b**), 15 s (**c**), 20 s (**d**) and 25 s (e)

In brief, one can identify three morphological structures at the micro and nanometric levels that constitute the Ag@ZnO/CA fibers prepared. At the micro level, we obtained ZnO fibers by providing sufficient sputtering time to cover the CA fibers. In addition, under limited adatom mobility, sputtered ZnO has columnar grain morphology at the nano level, which provides plenty of surface area for the adsorption of molecules. Regarding the Ag layer, nanoparticles were obtained by sputtering under limited adatom mobility and a short deposition time, i.e., 5 s. An important question for future studies is determining the substrate temperature effect on the size and shape of the Ag nanoparticles. As a proof of concept, we tested the Ag@ZnO/CA fibers as SERS substrates using BZT as the probe molecule.

3.3 Ag@ZnO/CA nanofibers as a SERS substrate

The SERS effect of the Ag@ZnO/CA fibers was studied using BZT as a probe molecule. Fig. 7a shows the SERS spectra in the 600 – 1800 cm^{-1} region of BZT adsorbed on the surface of ZnO/CA and Ag@ZnO/CA nanofibers sputtered with Ag for 5 seconds. The BZT Raman peaks were assigned following reported literature data [59]. No peaks of the dispersed BZT solution (10^{-3} M) on the ZnO/CA fibers could be observed. Conversely, four prominent peaks came forth for the BZT solution dispersed on the Ag@ZnO/CA fibers. The peak near 994 cm^{-1} is the carbon ring in-plane bending mode; the peak near 1016 cm^{-1} corresponds to the CH in-plane bending mode; the 1065 cm^{-1} peak is the carbon breathing mode, and the peak near 1567 cm^{-1} is the C=C stretching mode.

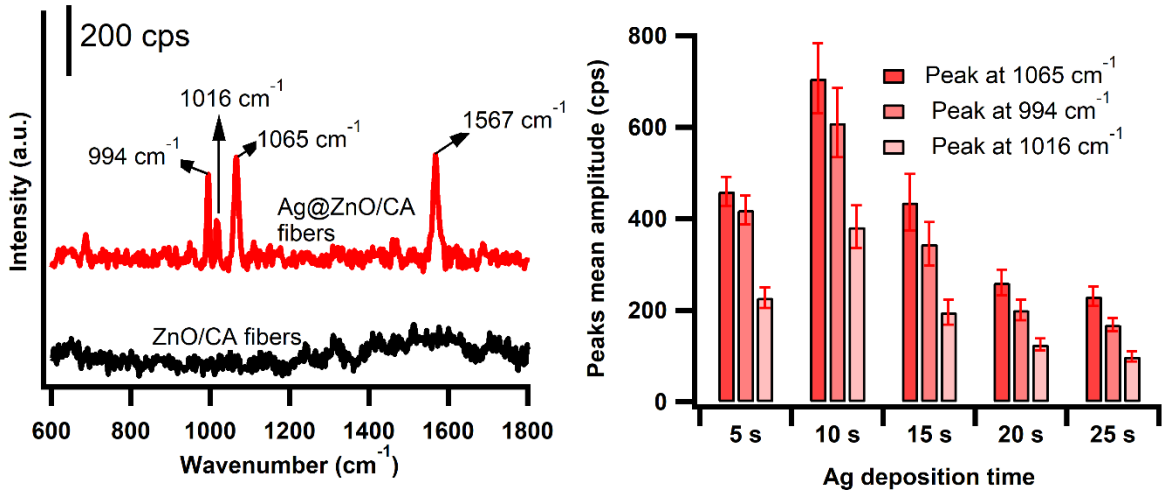

Fig. 7 SERS spectra of BZT adsorbed on ZnO/CA fibers (black) and Ag@ZnO/CA fibers (red) sputtered with Ag at a sputtering deposition time of 5 s (**a**). Peaks mean amplitude (**b**). The data in Fig. 7b are means ± 1 standard error (SE) (n=5)

Previous results on the SERS enhancement of sputtered Ag and Au nanoparticles revealed that extending the sputtering time raised the size and coverage of the nanoparticles. Such enhancement in size and surface coverage leads to a higher intensity of the SERS signal up to a particular value of sputtering time, followed by lower intensity values for a longer sputtering time [35,60]. To study the influence of the Ag sputtering time, we examined the intensity of the 994 cm^{-1}, 1016 cm^{-1}, and 1065 cm^{-1} peaks for the Ag@ZnO/CA fibers sputtered with Ag for 5, 10, 15, 20 and 25 seconds. Overall, the peaks mean amplitude increased when the sputtering deposition time extended from 5 to 10 s; then, a decrease in the mean amplitude, for 15 s, 20 s and 25 s sputtering time (Fig. 7b), is observed. The SERS intensity change with sputtering time observed agrees, in general, with the behavior reported in the works mentioned above. As discussed by Bo Li [35], increasing the size of the nanoparticles decreases the gaps between them, and the electromagnetic field intensifies in these regions, thus increasing the EM enhancement. However, if the size and surface coverage of the nanoparticles expands to develop a film structure, it reduces the number of gaps by filling these regions; as a result, the SERS enhancement diminishes.

In addition, to evaluate the reproducibility of the SERS signal of the Ag@ZnO/CA fibers with a 10 s AG deposition, we used BZT 10^{-3} M as the probe molecule as shown in Fig 8a. We randomly measured five spots on the same fiber and kept the same measurement conditions for each spot. We calculated the relative standard deviation (RSD) from the SERS spectra obtained at each spot. The estimated RSD was 11.6 %, which indicates that the SERS signal has good reproducibility. The substrate showed good reproducibility in the SERS measurements, which we attribute to two main factors. First, the successful coating of ZnO on the CA fibers by sputtering deposition under limited adatom mobility, resulted in a combined fiber morphology and columnar grain structure of the sputtered layers. This created a morphology with a large surface area for the BZT to adsorb and be detected by SERS. Second, the growth of Ag nanoparticles on top of ZnO, which generated a high density of SERS 'hot spots' between the nanoparticles and between the nanoparticles and ZnO. These 'hot spots' enhanced the electromagnetic field and increased the Raman signal of the BZT molecules.

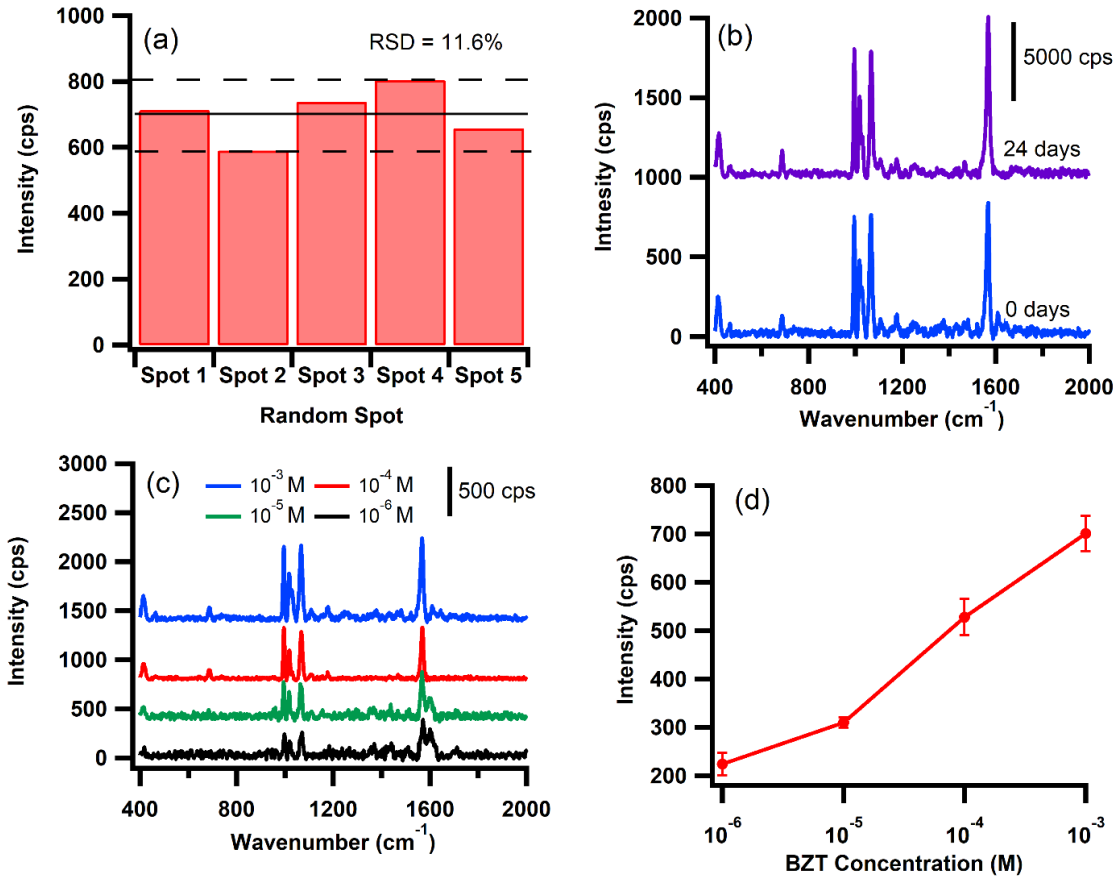

Fig. 8 Intensity distribution collected at five random spots of 1065 cm^{-1} peak of 10^{-3} M BZT on Ag@ZnO/CA fibers substrate with a 10 s Ag deposition. (**a**) SERS spectra of BZT adsorbed on Ag@ZnO/CA fibers collected at different shelf times. (**b**) SERS spectra of BZT adsorbed on Ag@ZnO/CA fibers obtained from different concentrations (10^{-3} M, 10^{-4} M, 10^{-5} M, 10^{-6} M). (**c**) 1065 cm^{-1} peak intensity vs BZT concentration. (**d**) The data points in Fig 8d are means ± 1 standard error (SE) (n=5)

One of the challenges for using SERS substrates in real-world scenarios is their stability over time. The SERS signal of BZT did not show any significant difference after 24 days compared to the signal from a new substrate (Fig. 8b). This suggests that Ag@ZnO is a stable SERS substrate that can be kept for almost a month at room temperature. A possible way to further improve the stability of our SERS substrate is to functionalize it with a bioinspired polymer, as suggested by a recent study [61]. The authors showed that polydopamine-coated aluminum nanocrystals could maintain their plasmonic properties in aqueous media for over two weeks, while uncoated nanocrystals rapidly oxidized and lost their functionality. We could apply a similar approach to our Ag@ZnO substrate and investigate how it affects the SERS signal of BZT and other probe molecules over time.

To evaluate the sensitivity of the SERS substrates, we selected Ag@ZnO/CA fibers with 10 s Ag deposition as the optimal condition based on the previous analysis. We performed SERS measurements for different concentrations of BZT ranging from 10^{-3} M to 10^{-6} M. The corresponding spectra are shown in Fig. 8c. The peak intensity at 1065 cm^{-1}, was used to quantify the SERS signal. As shown in Fig. 8d, the peak intensity decreased with a decrease of BZT concentration, but it was still clearly observable at 10^{-6} M level, indicating a high sensitivity of our substrates.

The Ag@ZnO/CA fibers (10 s Ag deposition) were further applied as the SERS substrate to detect R6G. We prepared a solution with 10^{-3} M R6G concentration and drop-casted it on the substrate. After drying in air, we obtained the SERS spectra in Fig. 9a, which shows the characteristic peaks of R6G. We observed five peaks of R6G at around 612 cm^{-1}, 771 cm^{-1}, 1360 cm^{-1}, 1506 cm^{-1} and 1650 cm^{-1}. According to the literature [43,62] , the peaks around 612 cm^{-1} and 771 cm^{-1} were assigned to in-plane and out-of-plane bending motions of the C-H bond, respectively, whereas the peaks at 1360 cm^{-1} and 1650 cm^{-1} are related to the C-C stretching mode of the aromatic ring.

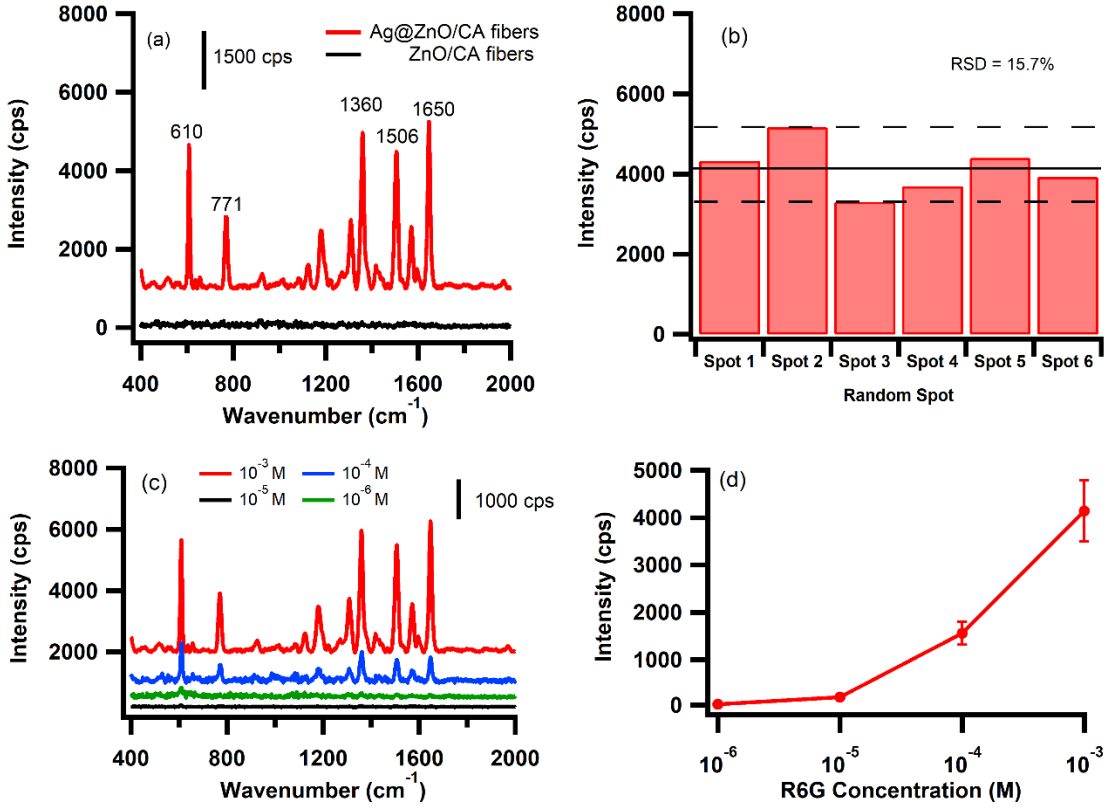

Fig. 9 SERS spectra of R6G adsorbed on ZnO/CA fibers (black) and Ag@ZnO/CA fibers (red) sputtered with Ag at a sputtering deposition time of 10 s (**a**) Intensity distribution collected at five random spots of 610 cm^{-1} peak of 10^{-3} M R6G on Ag@ZnO/CA fibers substrate with a 10 s Ag deposition. (**b**) SERS spectra of R6G adsorbed on Ag@ZnO/CA fibers obtained from different concentrations (10^{-3} M, 10^{-4} M, 10^{-5} M, 10^{-6} M). (**c**) 610 cm^{-1} peak intensity vs R6G concentration. (**d**) The data points in Fig 9c indicate mean intensity of peak 610 cm^{-1} of five measurements and the error bar represents the standard error of the mean.

The reproducibility of Ag@ZnO/CA fibers was also tested using R6G. We randomly measured six spots on the same fiber and estimated the relative standard deviation (RSD) from the SERS spectra obtained at each location. The estimated RSD was 16.6 %, indicating good signal reproducibility as in the cases of the BZT probe molecule. Lastly, we also observed the SERS signals with a low concentration, as shown in Fig. 9c and Fig. 9d. These results indicate that Ag@ZnO/CA fibers can detect R6G at a concentration as low as 10^{-6} M. The limit of detection Ag@ZnO/CA fibers towards R6G is comparable to other SERS substrates, such as TiN SERS substrates of various morphologies (nanoporous films [63] and nanorods arrays [64]).

All things considered, our findings demonstrate the feasibility of sputtering materials under limited adatom mobility conditions onto templates to obtain SERS substrates with various morphological structures at the micro and nanometric levels capable of detecting BZT and R6G at low concentrations.

4 Conclusions

By combining sputtering deposition and electrospinning technique, we developed a straightforward and effective method for preparing SERS substrate with various morphological structures at the micro and nanoscales. We successfully prepared Ag@ZnO/CA fiber composites by sputtering ZnO and Ag onto cellulose acetate fibers. The selected sputtering process parameters for the deposition of ZnO allowed reducing the adatoms' thermally induced mobility. Whereas for Ag, the sputtering parameters were selected so as to cut down the bombardment-induced and thermally-induced mobility. Under such limited adatom mobility, the cellulose acetate fibers were covered by ZnO columnar grains at the nanoscale. Moreover, under low adatom mobility and short deposition times, the Ag sputtering yielded nanoparticles of different sizes and shapes on the ZnO surface. All the synthesized composites rendered good SERS responses towards BZT. An improvement is observed for the composite prepared at an Ag deposition time of 10s. One can attribute this occurrence to an enhancement of the electromagnetic field due mainly to (a) small gaps between the Ag nanoparticles and (b) an increase in particle size. The Ag@ZnO/CA fiber composites with 10 s Ag deposition also shows good uniformity and response at low concentrations of BZT and R6G, which could be used for the detection of these probe molecules with a detection limit of 10^{-6} M. Our work offers a facile approach to produce Ag@ZnO/CA fibers that can be used as SERS sensors for various applications. This research also provided insight into the effects of limited adatoms mobility conditions on the morphological structure developed for the deposited Ag@ZnO composite at various length scales.

Acknowledgments

This work was supported by the National Science Foundation grants number 2112537 (NSF CREST Postdoctoral Research Fellowship) and 1345156 (NSF CREST Program). Infrastructure support by the UPRM Dean of Students Office is acknowledged by coauthor Suárez. The authors would like to thank the Material Characterization Center of the University of Puerto Rico (UPR) for electron microscopy services and Dr. Danilo Barrionuevo (UPR- Cayey campus) for his assistance in the profilometer measurements. The authors acknowledge the UPR-Cayey campus for the sputtering facilities. The authors acknowledge the UPR Molecular Science Research Center for the Raman and SERS measurements. We also kindly acknowledge Professors Marco De Jesus and Francisco Bezares for many helpful discussions about SERS. The authors would like to thank Dr. Wilfredo for his valuable and constructive suggestions during the revision process of the manuscript.

Declarations

Authors' contributions

All authors contributed to the technology's study, conception, and design. Materials preparation, data collection, and analysis were performed by Adrián Camacho-Berríos. Resources provided by Oscar Marcelo Suárez. Supervision of research activities by Oscar Marcelo Suárez. Project administration by Adrián Camacho-Berríos and Oscar Marcelo Suárez. The first draft of the manuscript was first composed by Adrián Camacho-Berríos Funding acquisition by Adrián Camacho-Berríos and Oscar Marcelo Suárez. The review and editing of the manuscript were

performed by Oscar Marcelo Suárez. All authors commented on previous versions of the manuscript. All authors read and approved the final manuscript.

Funding and/or Conflicts of interests/Competing interests

This work was supported by the National Science Foundation (Grants numbers 2112537 and 1345156).
The authors have no relevant financial or non-financial interests to disclose. The authors have no competing interests to declare relevant to this article's content.

Data availability

The datasets generated during and/or analyzed during the current work are available from the corresponding author upon reasonable request.

References

1. B. Zhao, H. Liu, L. Xia, Z. Wang, and C. Zhang, ACS Appl Nano Mater (2022).

2. L. Xie, K. Gong, Y. Liu, and L. Zhang, Environ Sci Technol (2022).

3. A. Hussain, H. Pu, B. Hu, and D. W. Sun, Spectrochim Acta A Mol Biomol Spectrosc **245**, (2021).

4. A. Hussain, H. Pu, and D. W. Sun, Journal of Food Measurement and Characterization **14**, 2021 (2020).

5. G. Beaton, Y. Bdour, C. Escobedo, and K. Stamplecoskie, ACS Appl Nano Mater (2022).

6. M. A. Fikiet, S. R. Khandasammy, E. Mistek, Y. Ahmed, L. Halámková, J. Bueno, and I. K. Lednev, Spectrochim Acta A Mol Biomol Spectrosc (2018).

7. B. Thirumalraj, Biomed J Sci Tech Res **16**, 0 (2019).

8. K. Kneipp, Phys Today 40 (2007).

9. F. Kretschmer, S. Mühlig, S. Hoeppener, A. Winter, M. D. Hager, C. Rockstuhl, T. Pertsch, and U. S. Schubert, Particle and Particle Systems Characterization **31**, 721 (2014).

10. X. M. Lin, Y. Cui, Y. H. Xu, B. Ren, and Z. Q. Tian, Anal Bioanal Chem **394**, 1729 (2009).

11. S. Barbosa, A. Agrawal, L. Rodríguez-Lorenzo, I. Pastoriza-Santos, R. A. Alvarez-Puebla, A. Kornowski, H. Weller, and L. M. Liz-Marzán, Langmuir **26**, 14943 (2010).

12. Q. Zhang, N. Li, J. Goebl, Z. Lu, and Y. Yin, J Am Chem Soc **133**, 18931 (2011).

13. Q. Xu, X. Guo, L. Xu, Y. Ying, Y. Wu, Y. Wen, and H. Yang, Sens Actuators B Chem **241**, 1008 (2017).

14. H. Im, K. C. Bantz, S. H. Lee, T. W. Johnson, C. L. Haynes, and S. H. Oh, Advanced Materials **25**, 2678 (2013).

15. D. Wang, W. Zhu, M. D. Best, J. P. Camden, and K. B. Crozier, Nano Lett **13**, 2194 (2013).

16. W. Zhu, M. G. Banaee, D. Wang, Y. Chu, and K. B. Crozier, Small **7**, 1761 (2011).

17. Z. B. Wang, B. S. Luk'yanchuk, W. Guo, S. P. Edwardson, D. J. Whitehead, L. Li, Z. Liu, and K. G. Watkins, Journal of Chemical Physics **128**, (2008).

18. K. Xu, H. Yan, C. F. Tan, Y. Lu, Y. Li, G. W. Ho, R. Ji, and M. Hong, Adv Opt Mater **6**, (2018).

19. Z. Sun, X. Fang, C. Kang, Y. Han, L. Zha, and X. Zhang, ACS Appl Nano Mater (2022).

20. S. Kalasung, I. Chatnuntawech, V. Patthanasettakul, S. Limwichean, K. Lertborworn, M. Horprathum, N. Nuntawong, P. Eiamchai, and K. Aiempanakit, in *Mater Today Proc* (Elsevier Ltd, 2021), pp. 3517–3524.

21. L. Xu, H. Zhang, Y. Tian, A. Jiao, F. Chen, and M. Chen, Talanta **194**, 680 (2019).

22. H. Chen, H. Liu, Y. Chen, X. Li, C. Gu, and T. Jiang, Mater Chem Phys **273**, (2021).

23. C. Huang, C. Xu, J. Lu, Z. Li, and Z. Tian, Appl Surf Sci **365**, 291 (2016).

24. C. Liu, X. Xu, C. Wang, G. Qiu, W. Ye, Y. Li, and D. Wang, Sens Actuators B Chem **307**, (2020).

25. Z. Zhao, H. Bao, Q. Zhao, H. Fu, L. Zhou, H. Zhang, Y. Li, and W. Cai, ACS Appl Mater Interfaces **14**, 47999 (2022).

26. Y. C. Lai, H. C. Ho, B. W. Shih, F. Y. Tsai, and C. H. Hsueh, Appl Surf Sci **439**, 852 (2018).

27. Q. Huang and J. Li, Mater Lett **204**, 85 (2017).

28. L. Chen, L. Luo, Z. Chen, M. Zhang, J. A. Zapien, C. S. Lee, and S. T. Lee, Journal of Physical Chemistry C **114**, 93 (2010).

29. F. Xu, Y. Zhang, Y. Sun, Y. Shi, Z. Wen, and Z. Li, Journal of Physical Chemistry C **115**, 9977 (2011).

30. Z. Yi, Y. Y. Yi, J. Luo, X. Li, X. Xu, X. Jiang, Y. Y. Yi, and Y. Tang, Physica B Condens Matter **451**, 58 (2014).

31. K. Sivashanmugan, J. der Liao, B. H. Liu, C. K. Yao, and S. C. Luo, Sens Actuators B Chem **207**, 430 (2015).

32. J. Huang, F. Chen, Q. Zhang, Y. Zhan, D. Ma, K. Xu, and Y. Zhao, ACS Appl Mater Interfaces **7**, 5725 (2015).

33. G. Zhang, C. Deng, H. Shi, B. Zou, Y. Li, T. Liu, and W. Wang, Appl Surf Sci **402**, 154 (2017).

34. X. Yuan, W. Xu, F. Huang, D. Chen, and Q. Wei, Appl Surf Sci **390**, 863 (2016).

35. B. Li, Y. E. Shi, J. Cui, Z. Liu, X. Zhang, and J. Zhan, Anal Chim Acta **923**, 66 (2016).

36. J. H. Park and Y. L. Joo, Appl Surf Sci **416**, 742 (2017).

37. L. Liu, P. Martinez Pancorbo, T. H. Xiao, S. Noguchi, M. Marumi, H. Segawa, S. Karhadkar, J. Gala de Pablo, K. Hiramatsu, Y. Kitahama, T. Itoh, J. Qu, K. Takei, and K. Goda, Adv Opt Mater **10**, (2022).

38. F. Lu, J. Wang, Z. Chang, and J. Zeng, Mater Des **181**, (2019).

39. D. Rodri´guez-Vindas, J Nanophotonics **2**, 021925 (2008).

40. P. Carvalho, P. Sampaio, S. Azevedo, C. Vaz, J. P. Espinós, V. Teixeira, and J. O. Carneiro, Appl Surf Sci **307**, 548 (2014).

41. A. N. Fouda, E. S. M. Duraia, and E. A. Eid, Superlattices Microstruct **73**, 268 (2014).

42. A. Ismail, M. J. Abdullah, and M. A. Qaeed, J Lumin **164**, 69 (2015).

43. N. Kaisar, Y. T. Huang, S. Jou, H. F. Kuo, B. R. Huang, C. C. Chen, Y. F. Hsieh, and Y. C. Chung, Surf Coat Technol **337**, 434 (2018).

44. E. Muchuweni, T. S. Sathiaraj, and H. Nyakotyo, Mater Res Bull **95**, 123 (2017).

45. M. Ohring, *The Materials Science of Thin Films* (Academic Press, San Diego, 1992).

46. Z. Li and W. Gao, Mater Lett **58**, 1363 (2004).

47. J. A. Thornton, in *J Vac Sci Technol* (1974), pp. 666–670.

48. R. Messier, A. P. Giri, and R. A. Roy, Journal of Vacuum Science & Technology A: Vacuum, Surfaces, and Films **2**, 500 (1984).

49. G. Guisbiers and S. Pereira, Nanotechnology **18**, (2007).

50. A. Salama, A. Mohamed, N. M. Aboamera, T. Osman, and A. Khattab, Advances in Polymer Technology **37**, 2446 (2018).

51. Z. Liu, T. Zhao, W. Fan, X. Men, K. Jiang, and G. Lu, ACS Appl Nano Mater **5**, 2280 (2022).

52. Ü. Özgür, Y. I. Alivov, C. Liu, A. Teke, M. A. Reshchikov, S. Doğan, V. Avrutin, S. J. Cho, H. Morkǫ, U. Ozgur, Y. I. Alivov, C. Liu, A. Teke, M. A. Reshchikov, S. Dogan, V. Avrutin, S. J. Cho, and H. Morkoç, J Appl Phys **98**, 1 (2005).

53. N. A. Putri, V. Fauzia, S. Iwan, L. Roza, A. A. Umar, and S. Budi, Appl Surf Sci **439**, 285 (2018).

54. H. B. Ruan, C. Y. Kong, G. P. Qin, W. J. Li, T. Y. Yang, F. Wu, and L. Fang, J Magn Magn Mater **369**, 219 (2014).

55. Q. Q. Gao, Q. X. Yu, K. Yuan, X. N. Fu, B. Chen, C. X. Zhu, and H. Zhu, Appl Surf Sci **264**, 7 (2013).

56. D. E. E. Motaung, I. Kortidis, D. Papadaki, S. S. S. Nkosi, G. H. H. Mhlongo, J. Wesley-Smith, G. F. F. Malgas, B. W. W. Mwakikunga, E. Coetsee, H. C. C. Swart, G. Kiriakidis, and S. S. S. Ray, Appl Surf Sci **311**, 14 (2014).

57. H. Ruan, L. Fang, W. Li, G. Qin, F. Wu, and C. Kong, Mater Sci Semicond Process **21**, 52 (2014).

58. T. H. Chang, Y. C. Chang, and S. H. Wu, J Alloys Compd **843**, (2020).

59. J. Song, W. Cheng, M. Nie, X. He, W. Nam, J. Cheng, and W. Zhou, ACS Nano **14**, 9521 (2020).

60. T. H. Chang, Y. C. Chang, and S. H. Wu, J Alloys Compd **843**, (2020).

61. D. Renard, S. Tian, A. Ahmadivand, C. J. Desantis, B. D. Clark, P. Nordlander, and N. J. Halas, ACS Nano **13**, 3117 (2019).

62. Y. Cao, P. Liang, Q. Dong, D. Wang, D. Zhang, L. Tang, L. Wang, S. Jin, D. Ni, and Z. Yu, Anal Chem (2019).

63. H. Wei, M. Wu, Z. Dong, Y. Chen, J. Bu, J. Lin, Y. Yu, Y. Wei, Y. Cui, and R. Wang, Journal of Raman Spectroscopy **48**, 578 (2017).

64. J. Zhao, J. Lin, H. Wei, X. Li, W. Zhang, G. Zhao, J. Bu, and Y. Chen, Opt Mater (Amst) **47**, 219 (2015).